OXFORD

SOT | Society of Toxicology
academic.oup.com/toxsci

TOXICOLOGICAL SCIENCES, 177(2), 2020, 506–520

doi: 10.1093/toxsci/kfaa115
Advance Access Publication Date: 21 July 2020
Research Article

NF-κB Signaling in Astrocytes Modulates Brain Inflammation and Neuronal Injury Following Sequential Exposure to Manganese and MPTP During Development and Aging

Sean L. Hammond,* Collin M. Bantle,* Katriana A. Popichak,* Katie A. Wright,* Delaney Thompson,* Catalina Forero,* Kelly S. Kirkley,* Pranav U. Damale,† Edwin K.P. Chong,† and Ronald B. Tjalkens*,[1]

*Toxicology Program, Department of Environmental and Radiological Health Sciences, College of Veterinary Medicine and Biomedical Sciences and †Department of Electrical and Computer Engineering, College of Engineering, Colorado State University, Fort Collins, Colorado 80523-1680

[1]To whom correspondence should be addressed at Toxicology Program, Department of Environmental and Radiological Health Sciences, College of Veterinary Medicine and Biomedical Sciences, Colorado State University, 1680 Campus Delivery, Physiology Building, Room 101, Fort Collins, CO 80523-1680. Fax: (970) 491-7569. E-mail: ron.tjalkens@colostate.edu.

ABSTRACT

Chronic exposure to manganese (Mn) is associated with neuroinflammation and extrapyramidal motor deficits resembling features of Parkinson's disease. Activation of astrocytes and microglia is implicated in neuronal injury from Mn but it is not known whether early life exposure to Mn may predispose glia to more severe inflammatory responses during aging. We therefore examined astrocyte nuclear factor kappa B (NF-κB) signaling in mediating innate immune inflammatory responses during multiple neurotoxic exposures spanning juvenile development into adulthood. $MnCl_2$ was given in drinking water for 30-day postweaning to both wildtype mice and astrocyte-specific knockout (KO) mice lacking I kappa B kinase 2, the central upstream activator of NF-κB. Following juvenile exposure to Mn, mice were subsequently administered 1-methyl-4-phenyl-1,2,3,6-tetrahydropyridine (MPTP) at 4 months of age. Animals were evaluated for behavioral alterations and brain tissue was analyzed for catecholamine neurotransmitters. Stereological analysis of neuronal and glial cell counts from multiple brain regions indicated that juvenile exposure to Mn amplified glial activation and neuronal loss from MPTP exposure in the caudate-putamen and globus pallidus, as well as increased the severity of neurobehavioral deficits in open field activity assays. These alterations were prevented in astrocyte-specific I kappa B kinase 2 KO mice. Juvenile exposure to Mn increased the number of neurotoxic A1 astrocytes expressing C3 as well as the number of activated microglia in adult mice following MPTP challenge, both of which were inhibited in KO mice. These results demonstrate that exposure to Mn during juvenile development heightens the innate immune inflammatory response in glia during a subsequent neurotoxic challenge through NF-κB signaling in astrocytes.

Key words: astrocyte; microglia; manganese; MPTP; inflammation; neurodegeneration.

Manganese (Mn) is an essential trace element necessary for multiple enzymatic processes in the central nervous system (CNS), where it is a required cofactor for enzymes important for neuronal health such as glutamine synthetase (GS), the key enzyme regulating glutamate-glutamine metabolic shuttling between astrocytes and neurons (Aschner *et al.*, 2009) and superoxide dismutase (Mn-SOD), which protects neurons from the damaging effects of oxidative stress (Zidenberg-Cherr *et al.*, 1983). Mn is highly concentrated in astrocytes, with cellular uptake mediated by divalent metal transporters such as DMT1, ZIP, and SLC39A3 (Aschner *et al.*, 2009). Elevated concentrations of Mn within astrocytes promote a neuroinflammatory phenotype, characterized by expression of numerous genes that cause neuronal injury, including inducible nitric oxide synthase (NOS2), C-C motif chemokine ligand 2 (Ccl2), tumor necrosis factor (Tnf), interleukin 1β (Il1b), and interleukin 6 (Il6) (Kirkley *et al.*, 2017; Popichak *et al.*, 2018).

Neurotoxic levels of Mn correlate with cognitive and behavioral impairment in both adults and children (He *et al.*, 1994; Rugless *et al.*, 2014; Takser *et al.*, 2003), with motor deficits occurring at higher exposures in occupational settings such as mining and welding that can cause Mn-induced parkinsonism or "manganism" (Racette *et al.*, 2017; Rodier, 1955; Wang *et al.*, 1989). Neurological symptoms of manganism include bradykinesia, dystonia, rigidity, and depression (Mergler and Baldwin, 1997; Racette *et al.*, 2017; Rodier, 1955; Wang *et al.*, 1989), although patients with manganism do not display severe nigrostriatal dysfunction or resting tremors and are typically nonresponsive to levodopa (L-DOPA) therapy. These differences are likely due to distinct patterns of neuropathology compared with idiopathic Parkinson's disease (PD), causing toxicity primarily in more glial rich regions, such as the globus pallidus (Gp), subthalamic nucleus (Sth), and substantia nigra *pars reticulata* (SNpr) (Guilarte *et al.*, 2006; Peres *et al.*, 2016). In contrast, PD is characterized by preferential loss of dopamine (DA) neurons in the substantia nigra *pars compacta* (SNpc) and long axonal projections to the striatum (ST). Despite these findings, mechanisms by which Mn exposure could accelerate PD-like neuropathology remain elusive.

We previously demonstrated that Mn-induced neurotoxicity results in marked activation in astrocytes and microglia and expression of numerous neuroinflammatory genes that potentiate neuronal injury (Kirkley *et al.*, 2017; Moreno *et al.*, 2011). Furthermore, we reported that mice pre-exposed to Mn during juvenile development had higher levels of gliosis and neuronal dysfunction than mice exposed to Mn only as adults (Moreno et al., 2009b). Neurotoxic levels of glial activation and neuroinflammation resulting from Mn exposure are modulated by the transcription factor nuclear factor kappa B (NF-κB), a central regulator of innate immune inflammatory responses in lymphoid and myeloid cells, as well as in microglia and astrocytes (Glass *et al.*, 2010; Kirkley *et al.*, 2017; Popichak *et al.*, 2018). NF-κB has distinct functions within different cell types of the CNS, including regulation of inflammatory gene expression in glia and induction of prosurvival genes in neurons including IAP's, Bcl2, Bcl-XL, and survivin (Glass *et al.*, 2010). *In vitro*, Mn directly activates microglia, stimulating NF-κB-dependent release of cytokines such as TNFα that stimulate a reactive neurotoxic phenotype in astrocytes (Kirkley *et al.*, 2017). NF-κB is activated by numerous intra- and intercellular stressors, including reactive oxygen species (ROS), inflammatory cytokines, and chemokines, as well as Mn accumulation (Moreno *et al.*, 2011; Popichak *et al.*, 2018).

To determine the role of NF-κB in regulating the neuroinflammatory effects of Mn in reactive astrocytes, we recently developed a novel transgenic mouse with astrocyte-specific deletion of the NF-κB signaling pathway (Kirkley *et al.*, 2019). Mice expressing Cre recombinase under control of the human glial fibrillary acidic protein promoter (hGFAP) were crossed with I kappa B kinase 2 (Ikk2)-loxP mice to ablate inflammatory NF-κB signaling in astrocytes. Selective deletion of IKK2 in astrocytes protected against loss of DA neurons caused by the neurotoxin, 1-methyl-4-phenyl-1,2,3,6-tetrahydropyridine (MPTP) (Kirkley *et al.*, 2019). Lack of functional NF-κB in astrocytes decreased reactive gliosis in this model and decreased expression of NOS2 and TNFα, thereby reducing neuronal apoptosis. These studies demonstrated that inflammatory activation of glial cells is an important determinant of MPTP neurotoxicity (Kirkley *et al.*, 2019). However, it is unknown whether exposure to Mn can exacerbate the effects of other dopaminergic neurotoxins such as MPTP by modulating glial reactivity and subsequent neuroinflammatory injury. Exposure to MPTP as model neurotoxicant was used to test the potential combinatorial effects of Mn with other mitochondrial inhibitors such as pesticides (Brown *et al.*, 2006) and drugs of abuse (Peres *et al.*, 2016) that could aggravate pathology within the nigrostriatal dopamine system. In this study, we postulated that Mn exposure during juvenile development would stimulate NF-κB-dependent activation of microglia and astrocytes, resulting in chronic neuroinflammation that increases susceptibility to neuronal injury from a secondary exposure to a dopaminergic neurotoxin during aging.

MATERIALS AND METHODS

Animals and treatment regimen. All animals were housed on a 12-h light/dark cycle in a temperature-controlled room (maintained at 22–24°C) and had access to standard chow/water *ad libitum*. Procedures were approved by Colorado State University Institutional Animal Care and Use Committee (IACUC) and were conducted in compliance of National Institute of Health guidelines. Astrocyte-specific knockout (KO) mice for IKK2 were generated as previously described (Kirkley *et al.*, 2019). Briefly, *hGfap-cre*$^{+/-}$ (Cat No. 004600; Jackson Laboratories) mice were backcrossed on a C57/BlJ6 background for 12 generations before crossbreeding with *Ikk2-loxP*$^{+/+}$ mice (donated by Professor Michael Karin, University of California, San Diego). Four generations of crossbreeding were conducted to acquire *hGfap-cre*$^{+/-}$/*Ikk2-loxP*$^{+/+}$ (KO). Littermates lacking Cre recombinase (*hGfap-cre*$^{-/-}$/*Ikk2-loxP*$^{+/+}$) were used as genotype controls for the study. At day P21, mice were administered $MnCl_2$ (50 mg/kg/day) by monitoring water intake and weight gain for 30 days. After P51, mice were placed back on normal drinking water for a period of 2 months. This dose of Mn recapitulates higher levels of intake during the postnatal period from contaminated drinking water and from soy-based formulas, as noted in recent studies (Beaudin *et al.*, 2017) and as we previously published (Moreno *et al.*, 2009b). MPTP-HCl (MedchemExpress; Monmouth Junction, New Jersey) was dissolved in sterile saline (0.9% $NaCl_2$) and administered by sc injection at 20 mg/kg for 4 doses over 1 week. Probenecid was administered by ip injection (100 mg/kg; Sigma) every other day for 1 week (4 dosages total), per our previously published protocol (Hammond *et al.*, 2018). Mice were aged an additional week after treatment with 1-methyl-4-phenyl-1,2,3,6-tetrahydropyridine and probenecid (MPTPp) before tissue collection.

Behavioral analysis. Two weeks before initial behavioral testing, all mice were acclimated to stress handling by methods closely adapted to previously established protocols (Gouveia and Hurst, 2013; Stuart and Robinson, 2015). Open field activity parameters were assessed using the Versamax behavior chambers with an infrared beam grid detection array (Accuscan Instruments, Inc, Columbus, Ohio) as previously reported (Hammond *et al.*, 2018; Kirkley *et al.*, 2019). Mice were monitored for 10 min under low ambient light in the presence of white noise. Animals were preconditioned 1 day prior to their first treatment and then assessed at day 0 (1st day of treatment) to establish a baseline, day 7, and day 14. Several behavioral parameters were collected and analyzed using Versadat Software (Accuscan Instruments, Inc) including total distance traveled, number of movements, time spent moving, time spent in the margin, and the number of rearing movements. Baseline values were subtracted from each measurement to calculate the change in performance over time relative to baseline at the start of the study period. Stride length was assessed via video recording mice freely walking a glass trackway (5 cm × 1 m) with 3 recordings obtained per mouse per assessment, as previously reported (Hammond *et al.*, 2018; Kirkley *et al.*, 2019). Gait parameters were analyzed using software written in Mathworks/MatLab Software (in collaboration with Dr Edwin Chong, Professor of Electrical and Computer Engineering, Colorado State University). The light/dark was switched 2 weeks prior to the onset of studies so that behavioral measurements were performed during the wake cycle.

Tissue processing. For immunohistochemical analysis: mice were anesthetized under deep isoflurane and transcardially perfused with 0.1-M PBS-cacodylate/heparin (10 U/ml) and 3% paraformaldehyde/PBS. Following decapitation, whole brains were dissected and stored in 3% paraformaldehyde/PBS overnight at 4°C. The next day, samples were transferred to a gradient of 15%–30% sucrose/PBS prior to cryosectioning and storage in cryoprotectant at −20°C until processed for tissue staining. For neurochemical detection of Mn^{2+} and catecholamines: mice were similarly anesthetized with isoflurane and then rapidly decapitated. Whole brains were dissected and placed on a 1-mm brain block for separation of ST, SN, hypothalamus (Hyp), and cortex (Cx). Specific brain regions were frozen in liquid nitrogen and then stored at −80°C until processed for high-performance liquid chromatography (HPLC) and inductively coupled plasma-mass spectrometry (ICP-MS). Blood was also collected and centrifuged at (1500 rpm at 4°C/15 min) for plasma fractionation and stored at −80°C.

Immunostaining and automated stereological cell counting for fixed mouse brain tissue. For stereological determination of TH^+ neurons within the SN, the entire SNpc was serially cryosectioned from the Sth (rostral) to the retrorubal field (caudal) region. Every 6th free-floating section (8 total) was selected from each animal and immunostained for anti-TH (1:500; Millipore AB152) and anti-Neuronal Nuclei (NeuN; 1:250, Millipore; MAB377) by our previously reported protocol (Hammond *et al.*, 2018; Miller *et al.*, 2011). SNpc neurons were automatically quantitated from 10×-objective montage images of each immunostained section using a Hamamatsu ORCA-Flash4.0 digital CMOS camera, ProScan III stage controller (Prior, Rockland, Massachusetts) and CellSens Dimension Software (version 1.12, Olympus, Center Valley, Pennsylvania). For automated relative counts of $GFAP^+$, IBA-1^+, and $NeuN^+$ cells, 2 sections/animal were selected from the same anatomical regions of SN and ST (4 animals were analyzed per group). Primary antibodies for glia labeling were anti-GFAP (1:500; DAKO Z0334), anti-IBA1 (1:250; WAKO 016-20001), and anti-TH (Abcam 76442) to demarcate the SNpc and SNpr nuclei. Region of interest was highlighted based on Allen Brain Atlas for reference, following application of an adaptive threshold with shape factor and area (m^2) object filters for automatic cell detection, based on previously published algorithms (Tapias *et al.*, 2013). Detected cell number was divided over the area (μm^2) of region. The investigator was blinded from all experimental groups during imaging and cell quantification.

Image analysis of microglia morphology and reactive astrocytes. For detection of microglia morphology, the same sections immunostained for anti-IBA1/TH for automated counting were reimaged on a Zeiss Axiovert 200-M inverted wide-field fluorescence microscope equipped and a Hamamatsu ORCA-ER-cooled charge coupled device camera using a 10× and 40× Planapochromat air objectives with Slidebook imaging software (version 5.0, Intelligent Imaging Innovations, Denver Colorado). Optical fractionator method employed counting frame size (150 × 150 μm) and frame spacing (for SN; 250 × 250 μm, for ST; 550 ×550 μm); 40× z-stack images of IBA^+ cells from the SNpc, and Gp were acquired and converted to maximum projection, following a binary transformation and then rendered to a skeletonized image in ImageJ, as previously described (Morrison and Filosa, 2013; Schneider *et al.*, 2012). To detect expression of C3 in $S100\beta^+$ astrocytes, the same optical fractionator method was applied for imaging. Cells were manually quantified based on z-stack images. The investigator was blinded from all experimental groups during cell counting.

Analytical determination of catecholamines, monoamine, and manganese. Flash-frozen samples of brain tissue were processed for HPLC coupled with electrochemical detection to quantitate levels of dopamine (DA), 3,4-dihydroxyphenylacetic acid (DOPAC), homovanillic acid (HVA), serotonin (5-HT), and metabolite 5-hydroxindoleacetic acid (5-HIAA). The Neurochemistry Core Laboratory at Vanderbilt University's Center for Molecular Neuroscience Research (Nashville, Tennessee) processed all tissue samples from each experimental group with coded labeling for unbiased analysis. Levels of Mn in serum and brain were determined by ICP-MS through the metals analytical core facility at Vanderbilt University School of Medicine, as previously reported (Moreno *et al.*, 2009b).

Evaluation of mRNA expression by qPCR. RNA was isolated from brain tissue flash-frozen in liquid nitrogen and stored at −80°C utilizing the RNeasy Mini Kit (QIAGEN, Valencia, California). Purity and concentration were determined using a NanoDrop ND-1000 spectrophotometer. Five hundred ng of RNA was used as a template for reverse transcriptase reactions using the iScript RT kit (Bio-Rad, Hercules, California). cDNA was mixed with SYBR Green (Bio-Rad) and analyzed as previously reported (Kirkley *et al.*, 2017), utilizing primer pairs for *Slc11a2* (*Dmt1*), *Slc39a8* (*Zip8*), *Slc39a10*, and *Slc39a14*. Primer sequences were as follows: *Dmt1* (Forward: 5′ CAG CGA GAC TTG GAG TGG TC 3′, Reverse: 5′ CAC AGG ATG ATC CGT GGG A 3′), *Zip8* (Forward: 5′ ATC TGC CCC GCG ATC TTA C 3′, Reverse: 5′ CCC CAG ACT TCG GAA AGA CT 3′), *Slc39a10* (Forward: 5′ GGC CGT TAC TCA GGC AAG AC 3′, Reverse: GCA TGT TGA ACG AGT CCG AGA), and *Slc39a14* (Forward: 5′ CGC CAT TGA AGT ATG GGG GTA 3′, Reverse: 5′ GCA GGA GCC TCT TGT AAA AAG T 3′).

Statistical analysis. All data were presented as mean ± SEM, unless otherwise noted. Experimental values from each mean

were analyzed with a Grubb's ($\alpha = .05$) test for exclusion of significant outliers. Differences between genotype and treatment condition in each experimental group were analyzed by 2-way ANOVA with Tukey's post hoc multiple comparisons test. Significance was identified as $^{*}p < .05$, $^{**}p < .01$, $^{***}p < .001$, $^{****}p < .0001$. All statistical analysis was conducted using Prism (version 6.0; GraphPad Software, San Diego, California).

RESULTS

Developmental Weights and Water Consumption During Treatment With $MnCl_2$

At postnatal day (PND) 7 mice were tail clipped for DNA purification and identification of KO and wildtype (WT) progeny per our previously published PCR genotyping protocol (Kirkley *et al.*, 2019). From PN 21 to 51, encompassing the period of juvenile development to early adulthood, mice were placed on drinking water containing $MnCl_2$ (50 mg/kg/day) prior to later exposure to MPTPp, as depicted in Figure 1A. Based on statistical analysis of $MnCl_2$ water consumption, WT consumption increased 2.19 ± 0.44 (ml) and KO consumption increased 2.63 ± 0.78 (ml) from 21 to 51 PND ($n = 4$–5; no significance difference between groups) (Figure 1B). For accurate dosing of $MnCl_2$ and detection in change of body weight, mice were weighed every day for the 1st week of treatment. From 21 to 27 PND, WT and KO animals significantly increased in weight by 10.65 ± 0.97 and 10.86 ± 0.83 (g), respectively ($n = 8$/group; $^{****}p < .0001$). No significant difference in body weight was detected between WT and KO groups treated with $MnCl_2$ (Figure 1C). Mn levels in serum and brain were determined at the conclusion of Mn treatment at PN 51, as well as after treatment with MPTP in adult mice. At PN 51, there were increased levels of Mn in WT mice in the substantia nigra (SN), striatum (caudate-putamen, Cp) and cortex, with no increase in Mn evident in KO mice (Figs. 1D–F). There were no differences in Mn in serum between treatment groups in WT or KO mice (Figure 1G). In addition, Mn levels in brain and serum were not different from control following treatment with MPTPp alone in either genotype (data not shown). To understand potential differences in expression of metal transporters between WT and KO mice, we also measured mRNA expression of *Slc11a2* (*Dmt1*), *Slc39a8* (*Zip8*), *Slc39a10*, and *Slc39a14* (Figs. 1H–M). No changes in expression of *Dmt1*, *Slc30a10*, or *Slc39a14* were detected in the SN of mice between genotypes, either in control mice or in those treated with Mn or Mn + MPTPp (Figs. 1H–J). Levels of these transporters were likewise not different in the cortex between WT and KO mice, with the exception that *Dmt1* was somewhat increased in the cortex of KO mice treated with Mn + MPTPp (Figure 1K). Expression of mRNA for *Slca8* was not detected in any brain region evaluated.

Inhibition of NF-κB in Astrocytes Protects DA Neurons From MPTP-induced Toxicity in the SNpc

To determine the extent of neuronal loss in WT and KO mice following exposure to Mn and MPTP, the SN of each animal was serially cryosectioned and immunolabeled with anti-TH and anti-NeuN antibodies to label dopaminergic and total neurons, respectively (Figs. 2A–F). The total number of TH^+ neurons within the SNpc was quantitated for each experimental animal group as follows: WT control (8024 ± 637.1), WT with $MnCl_2$ (8779 ± 777.0), WT with MPTPp (3759 ± 503.7), WT with $MnCl_2$ + MPTPp (3867 ± 222.1), KO with MPTPp (7421 ± 537.2), KO with $MnCl_2$ + MPTPp (6957 ± 1049). Both WT with MPTPp and with $MnCl_2$ + MPTP displayed 51%–53% loss of TH^+ neurons compared with control. KO with MPTPp and $MnCl_2$ + MPTPp had only 7.5%–13.3% loss of TH^+ neurons (Figure 2G). The mean estimate of total $NeuN^+$ neurons within the SNpc was quantitated as follows: WT control ($14\ 034 \pm 631.2$), WT with $MnCl_2$ ($15\ 162 \pm 609.8$), WT with MPTPp (9778 ± 379.3), WT with $MnCl_2$ + MPTPp (9636 ± 159.0), KO with MPTPp ($12\ 932 \pm 1167$), KO with $MnCl_2$ + MPTPp ($11\ 695 \pm 1152$). Comparably, WT with MPTPp and $MnCl_2$ + MPTPp each had a similar 30%–31% loss of total neurons compared with control. KO with MPTPp and $MnCl_2$ + MPTPp only sustained a 7.8%–16.7% loss of $NeuN^+$ cells which was not significantly different from control (Figure 2H) ($n = 6$ animals/per group; $^{**}p < .01$, $^{***}p < .001$). $MnCl_2$ did not potentiate loss of dopaminergic neuronal soma following later exposure to MPTPp.

$MnCl_2$ Potentiates MPTPp-induced Neuronal Cell Death in the Gp and Striatum Activation of NF-κB in Astrocytes

To evaluate level of neuronal dysfunction in other basal ganglia nuclei affected by Mn, anatomically registered cryosections of the basal ganglia were selected for quantitation of total $NeuN^+$ neurons in the Gp and striatum (Cp). Representative montage images of sections immunolabeled with anti-NeuN (green) are depicted in Figures 3A–D. The Gp (Figure 3B) and Cp (Figure 3C) were highlighted as regions of interest (ROIs, highlighted in blue) for automated quantitative detection of the total number of $NeuN^+$ neurons per area (μm^2), with individual cell bodies visible in high magnification insets within each ROI. Based on quantitation of total $NeuN^+/\mu m^2$, there was an apparent decrease the number of neurons in WT animals treated with MPTPp or $MnCl_2$ individually, but this trend was not statistically different from control. In contrast, WT animals treated with $MnCl_2$ + MPTPp had a 44.1% loss of $NeuN^+$ neurons within the Gp and KO animals with dual treatment were protected from loss of neurons, with no differences in neuronal numbers detected compared with WT control animals (Figure 3E). Quantitation of $NeuN^+$ cells/μm^2 within the Cp showed a similar trend as the Gp, however no groups were statistically different (Figure 3F). To measure the integrity of TH^+ presynaptic terminals in the Cp, sections were also coimmunolabeled with anti-TH (red) as depicted in Figure 3D. An apparent decrease in TH^+ terminal density in WT animals treated with $MnCl_2$ or MPTPp individually was noted but was not significantly different from control. Dual treatment with both $MnCl_2$ and MPTPp in WT mice caused a decrease in DA terminal density to 62.5% of control animals, whereas KO animals with dual treatment only had a 20.7% loss of terminals compared with control WT mice (Figure 3G) ($n = 6$–7 animals/group; $^{*}p < .05$, $^{**}p < .01$, $^{***}p < .001$).

IKK2 KO Mice Are Protected Against Behavioral and Neurochemical Deficits Caused by Exposure to Mn and MPTPp

Spontaneous locomotor activity was detected by open field test (OFT) for each experimental group. In adult WT mice treated only with $MnCl_2$ as juveniles, there was a decrease in the total distance traveled but other behavioral parameters were unchanged from baseline (Figure 4A). In contrast, dual-treated WT mice ($MnCl_2$/MPTPp) displayed hyperactive behavior in multiple parameters of OFT analysis. Dual treatment significantly increased levels of margin time (Figure 4B), center time (Figure 4C), horizontal movement (Figure 4E), stereotypy movement (Figure 4F), and ambulatory movement (Figure 4G) compared with MPTPp-only treatment. Interestingly, treated KO animals did not display hyperactive behavior and were not

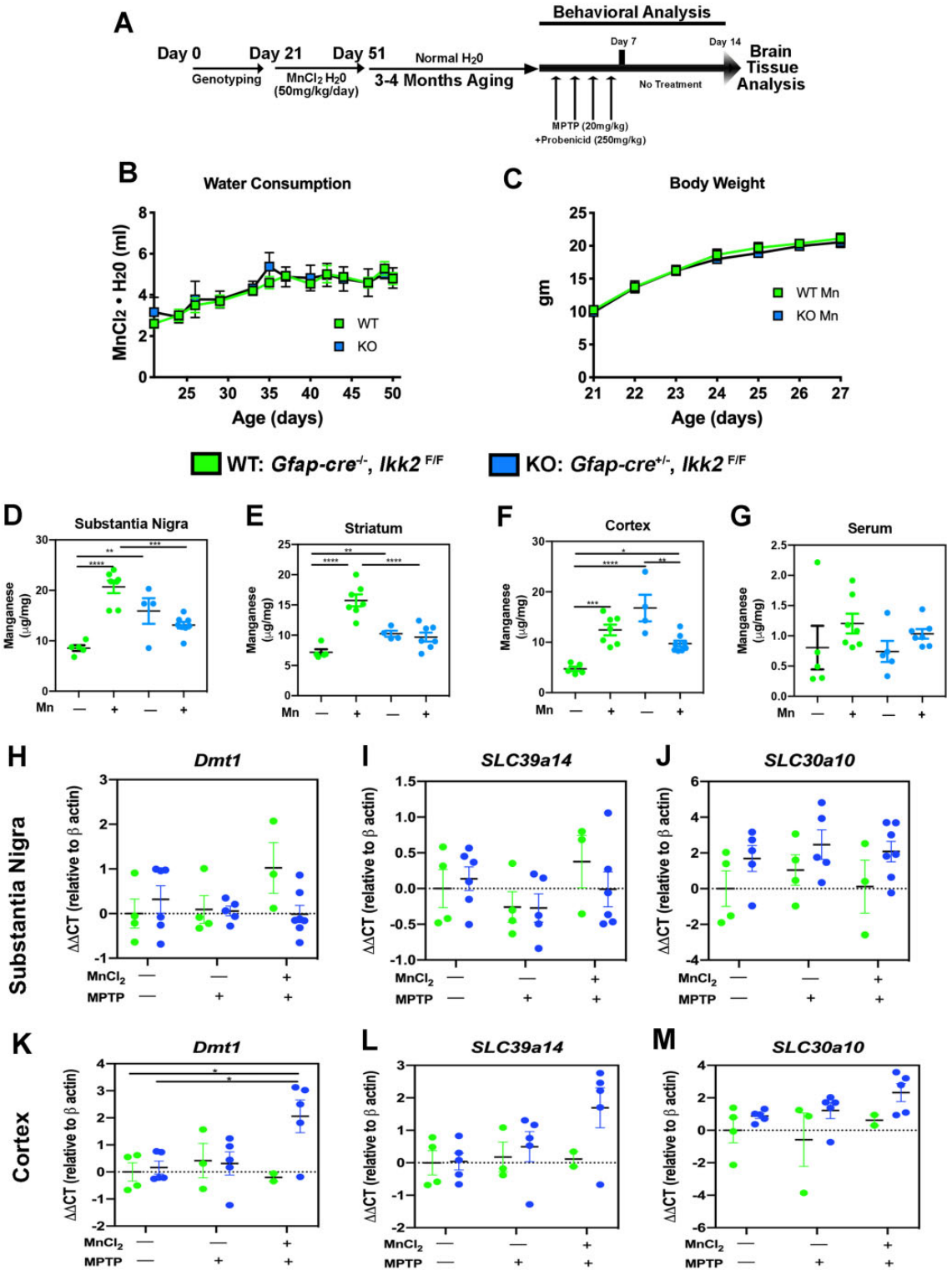

Figure 1. Treatment strategy and metal transporter expression for the 2-hit neurodegenerative model with manganese and 1-methyl-4-phenyl-1,2,3,6-tetrahydropyridine (MPTP). A, Experimental design for 2-hit neurodegenerative model. Wildtype (WT) (*Gfap-cre*$^{-/-}$, *Ikk2*$^{F/F}$) and astrocyte-specific knockout (KO) (*Gfap-cre*$^{-/-}$, *Ikk2*$^{F/F}$) mice were given either normal drinking water (18 Ω Milli-Q) or $MnCl_2{\cdot}4H_2O$ in drinking water (50 mg/kg/day Mn) from PN 21 to 51, followed by treatment with either vehicle or MPTP 4 months later. Behavioral analysis was conducted throughout the period of treatment with MPTP after collecting baseline data prior to dosing. All mice were terminated 1 week after the final dose of MPTP for analysis of neurochemical and immunohistochemical endpoints. B, Consumption of water and (C) body weight was not different between WT and KO mice exposed to $MnCl_2{\cdot}4H_2O$ in drinking water. Levels of Mn were measured at PN 51 in the substantia nigra (SN) (D), striatum (E), Cortex (F), and in serum (G). Expression of mRNA for metal transporters was determined in the SN (H–J) and cortex (K–M) of mice exposed to Mn or to Mn + MPTP at 6 months of age, relative to untreated control animals. $^{*}p < .05$, $^{**}p < .01$.

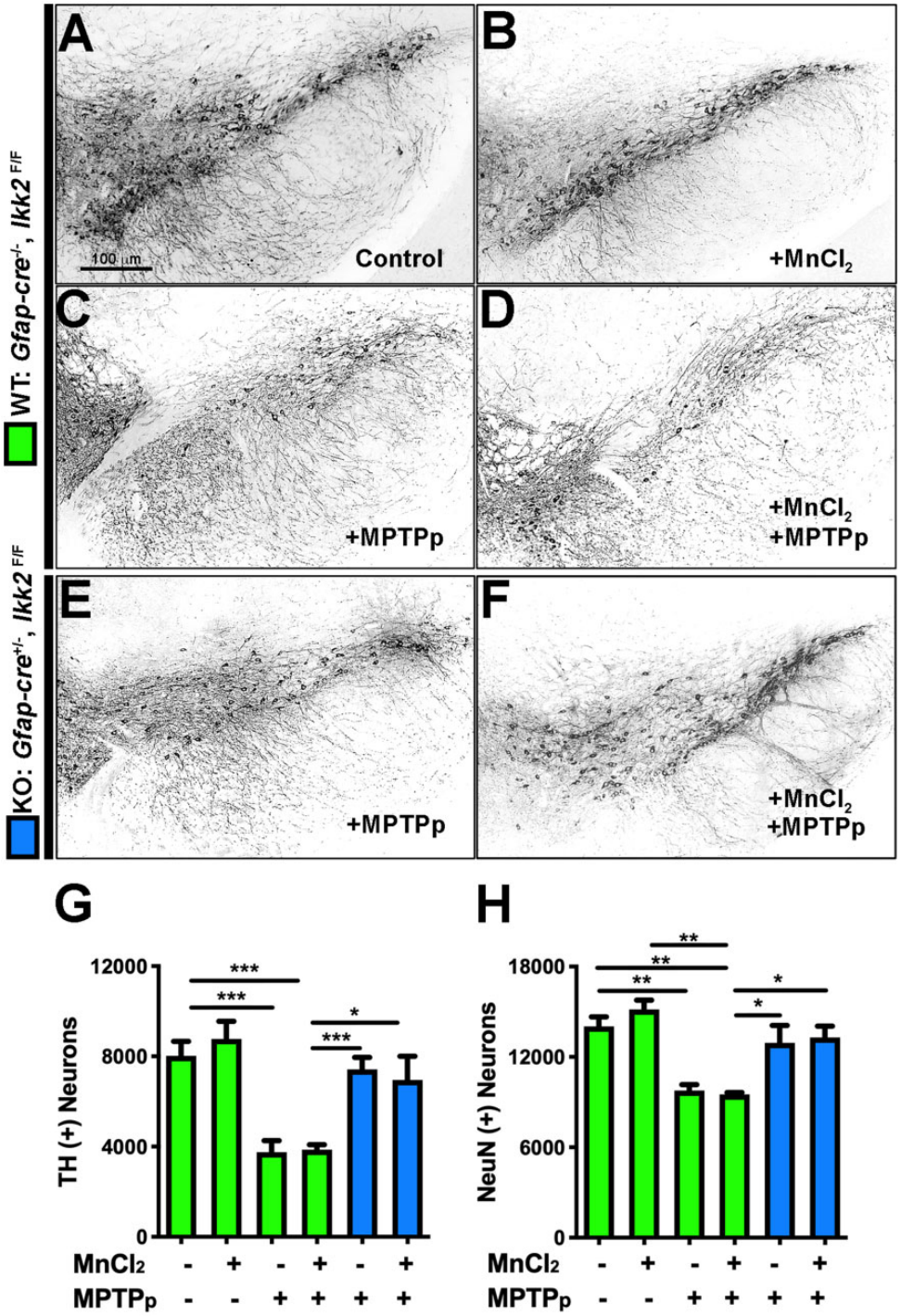

Figure 2. Astrocyte-specific knockout (KO) of I kappa B kinase 2 (IKK2) prevents loss of dopaminergic neurons following combined treatment with manganese and 1-methyl-4-phenyl-1,2,3,6-tetrahydropyridine (MPTP). The number of NeuN$^+$ (total) and tyrosine hydroxylase + (dopaminergic) neurons in the substantia nigra was determined by 3D designed-based stereology in frozen serial sections from wildtype (WT) (*Gfap-cre*$^{-/-}$/*Ikk2*$^{F/F}$) and KO (*Gfap-cre*$^{+/-}$/*Ikk2*$^{F/F}$) mice. Mice received either regular drinking water or drinking water containing 50 mg/kg/day $MnCl_2$ from PN 21 to 51 and were then treated with 1-methyl-4-phenyl-1,2,3,6-tetrahydropyridine and probenecid (MPTPp) or vehicle at 6 months of age. Dual-labeled immunofluorescence montage images were collected using a 10× air Plan Apochromat objective, counterstained DAPI to identify cell nuclei. Grayscale images of TH labeling are presented for each treatment group as follows: (A) WT—Control, (B) WT—$MnCl_2$, (C) WT—MPTPp, (D) WT—$MnCl_2$/MPTPp, (E) KO—MPTPp, (F) KO—$MnCl_2$/MPTPp. (G) Quantitative assessment of TH$^+$ neurons in the SNpc. (H) Quantitative assessment of total NeuN$^+$ neurons in the SNpc. $^{**}p < .01$, $^{***}p < .001$; $N = 6$ animals/group.

different from WT control animals, as depicted by the graphs in Figures 4A–C and 4E–G, as well as in representative traces and pseudocolored time plots of activity over a 5 min interval (Figure 4D) ($n = 7$–10 animals/group; $^{*}p < .05$, $^{**}p < .01$, $^{***}p < .001$, $^{****}p < .0001$). Quantitative analysis of stride length from each experimental animal was conducted using a real-time video gait analysis system. WT animals treated with MPTPp and $MnCl_2$/MPTPp exhibited an apparent decrease in stride length

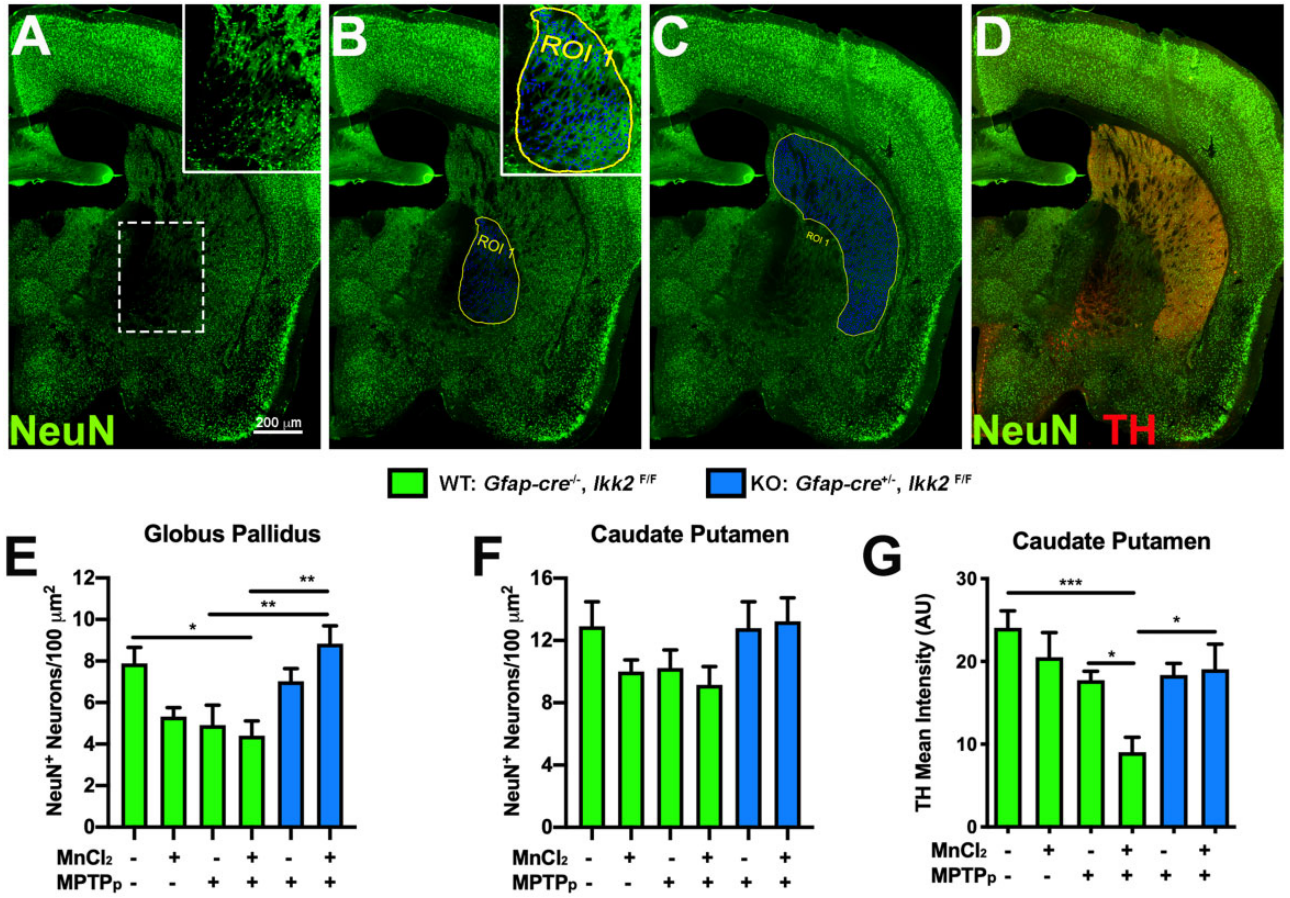

Figure 3. Sequential exposure to $MnCl_2$ and 1-methyl-4-phenyl-1,2,3,6-tetrahydropyridine (MPTP) causes neuronal loss in the globus pallidus (Gp) and enhances loss of dopaminergic fibers in the striatum through an astrocyte-dependent mechanism. Image analysis of $NeuN^+$ neurons the Gp and caudate-putamen (Cp) in wildtype (WT) and astrocyte-specific I kappa B kinase 2 (IKK2) knockout (KO) mice. A–D, Total neurons were immunolabeled with $NeuN^+$ (green) and sections were counterstained with TH (Red) to highlight dopaminergic terminals in the Cp (D). Regions of interest (ROIs) were drawn around each anatomically distinct nucleus for quantification of the total number of neurons. The Gp (B) and Cp (C) were identified as ROIs for automated cell detection (blue). Colabeling with anti-TH (red) depicts DA presynaptic terminals in the Cp (D). The total number of $NeuN^+$ cells/100 μm^2 was quantitated for the Gp (E) and Cp (F). G, Mean intensity of TH^+ immunoreactivity was measured for detection of DA innervation in the Cp. Juvenile exposure to Mn did not potentiate MPTP-induced neuronal loss in the Gp but did enhance MPTP-mediated loss of TH fibers in the Cp. $^*p < .05$, $^{**}p < .01$, $^{***}p < .001$; $N = 6–7$ animals/group. Abbreviation: MPTPp, 1-methyl-4-phenyl-1,2,3,6-tetrahydropyridine and probenecid.

compared with WT control that was not statistically significant. However, dual-treated KO animals had a significantly longer stride length compared with treated WT animals during the course of the study (Figure 4H) ($n = 5–6$ animals/group; $^*p < .05$).

Levels of striatal catecholamines and metabolites were detected by HPLC analysis with electrochemical detection. All MPTPp-treated animals with or without $MnCl_2$ exhibited a drastic loss of DA and DOPAC. In addition, a slight increase in DA levels was apparent in $MnCl_2$-only treated WT animals but was not statistically different from control (Figs. 4I and 4J). Dual-treated WT animals also displayed a significantly higher ratio of DOPAC/DA compared with control (Figure 4K). The DA metabolite, HVA, was also decreased with MPTPp treatment, independent of $MnCl_2$ treatment and genotype (Figure 4L). Serotonin (5H-T) content showed no statistical difference between experimental groups (Figure 4M). However, analysis of the serotonin metabolite (5-HIAA) showed a significant increase in both WT and KO dual-treated animals compared with MPTPp-only treatment (Figure 4N) ($n = 5–9$ animals/group; $^*p < .05$, $^{**}p < .01$, $^{***}p < .001$).

Juvenile Exposure to $MnCl_2$ Intensifies Activation of Microglia in the Gp After Treatment With MPTPp and Is Suppressed in Astrocyte-specific IKK2 KO Mice

The relative number of microglia within basal ganglia was detected by immunolabeling with anti-IBA1 as depicted in representative images of the Gp and Cp (Figs. 5A–C). Both MPTPp and MPTPp/$MnCl_2$ treatments in WT animals increased the number of $IBA\text{-}1^+$ cells/μm^2 within the Cp and treated KO animals displayed similar numbers as the control group, shown in Figure 5D. Dual-treated WT animals also exhibited the most $IBA\text{-}1^+$ cells/μm^2 within the Gp, which was reduced in KO animals (Figure 5E) ($n = 5–6$ animals/group; $^{**}p < .01$, $^{***}p < .001$, $^{****}p < .0001$). There was a significant increase in $IBA\text{-}1^+$ cells/μm^2 in the SNpc of MPTPp-treated WT animals and slightly less in KO animals, which was not statically different from WT (Figure 5F). A similar trend of $IBA\text{-}1^+$ cells/μm^2 in the SNpr was noted, although not statically different between groups (Figure 5F). For assessment of microglia morphology, 40×-objective IBA-1 (grayscale) images of the Cp and Gp were skeletonized to detect for number of branches as depicted in representative images in Figure 5H. WT dual-treated animals

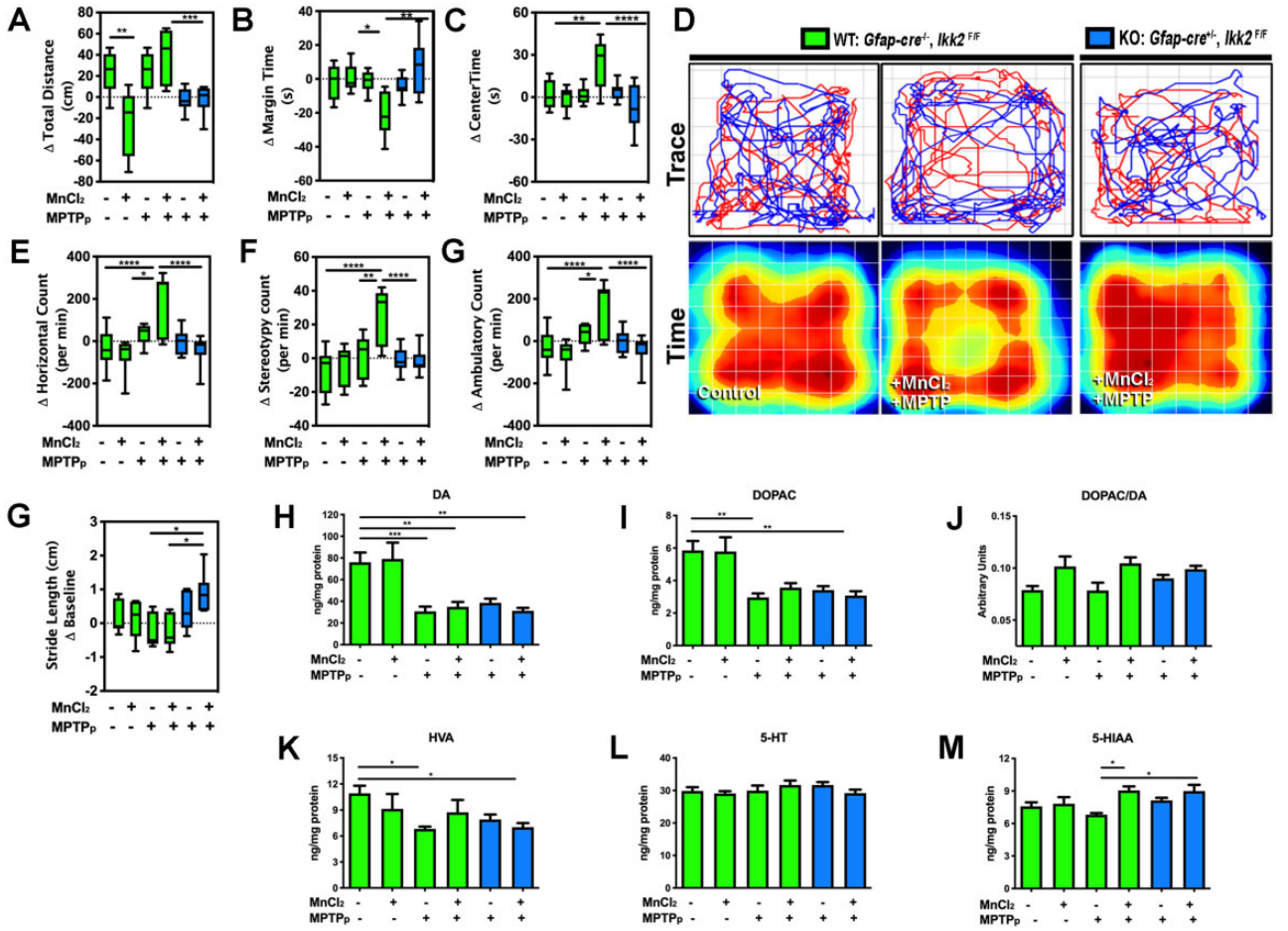

Figure 4. Juvenile exposure to manganese exacerbates 1-methyl-4-phenyl-1,2,3,6-tetrahydropyridine (MPTP)-induced behavioral dysfunction through NF-κB signaling in astrocytes. Open field behavioral testing for locomotor function was conducted for total distance (A), margin time (B), and center time (C), compared with baseline values prior to dosing with 1-methyl-4-phenyl-1,2,3,6-tetrahydropyridine and probenecid (MPTPp). D, Representative trace plots (top) and pseudocolored heat maps of total time spent (bottom) in the position of the chamber for 5 min intervals are depicted for (wildtype) WT—control, WT—$MnCl_2$/MPTPp, and (knockout) KO—$MnCl_2$/MPTPp animals. (E) Change in horizontal count, (F) stereotypy count, and (G) ambulatory count values were normalized to day 0 baseline values ($^*p < .05$, $^{**}p < .01$, $^{***}p < .001$, $^{****}p < .0001$; $N = 7$–10 animals/group). H, Real-time video gait analysis was utilized to quantitate change of stride length from day 0 ($^*p < .05$; $N = 5$–6 animals/group). High-performance liquid chromatography analysis was used for detection of neurotransmitter content from striatal tissue for (H) dopamine (DA), (I) 3,4-dihydroxyphenylacetic acid (DOPAC), (J) DOPAC/DA, (K) homovanillic acid (HVA), (L) serotonin (5-HT), and (M) 5-hydroxindoleacetic acid (5-HIAA) ($^*p < .05$, $^{**}p < .01$, $^{***}p < .001$; $N = 5$–6 animals/group).

exhibited significantly less branches/cell in the Cp (Figure 5I), Gp (Figure 5J), and less junctions/cell in the Cp (Figure 5K), and Gp (Figure 5K) compared with dual-treated KO animals ($n = 7$ animals/group; $^*p < .05$).

Activation of Astrocytes in the Basal Ganglia Following Dual Treatment With $MnCl_2$ and MPTPp Is Regulated by NF-κB

Expression of IKK2 was determined in hGfap-cre$^{+/-}$/Ikk2$^{fl/fl}$ mice by coimmunolabeling with anti-GFAP (red) and anti-IKK2 (green), as depicted in representative 100×-objective images from the Gp in WT control (Figure 6A), WT dual-treated (Figure 6B), and KO dual-treated (Figure 6C) mice. Expression of IKK2 protein was present in both control- and dual-treated WT mice but not detected in any experimental group of KO mice, similar to what we previously reported in astrocytes with these transgenic mice (Kirkley *et al.*, 2019). To assess the relative number of GFAP$^+$ cells in multiple nuclei of each experimental group, anatomically consistent cryosections of ST and SN were selected for automated counting of GFAP$^+$ cells/μm^2. As depicted in representative 10× montage images of the Gp and Cp, dual-treated WT animals exhibited increased proliferation of GFAP$^+$ astrocytes in both nuclei (Figure 6F). Dual treatment significantly increased the number of GFAP$^+$ cells in the Gp over MPTPp-only treatment in WT animals, which was markedly reduced in KO animals (Figs. 6D–G). Similarly, an increased number of GFAP$^+$ cells was evident in dual-treated WT animals in the Cp but was not statistically different from WT animals treated only with MPTPp in this region (Figure 6H). Comparably, dual-treated WT animals exhibited the greatest amount of GFAP$^+$ immunoreactivity in the SNpc, whereas KO animals had similar numbers of GFAP$^+$ cells as control mice (Figs. 6I–L) ($n = 6$; $^*p < .05$, $^{**}p < .01$, $^{***}p < .001$, $^{****}p < .001$). We also observed an apparent trend of GFAP$^+$ cells in the SNpr of each experimental group that was not statistically significant (Figure 6M).

Complement Protein-C3 Is Highly Expressed in Reactive Astrocytes Following Treatment With $MnCl_2$/MPTPp and Downregulated in IKK2 KO Mice

To quantitate number of neurotoxic astrocytes present throughout the basal ganglia, brain sections were stained for expression

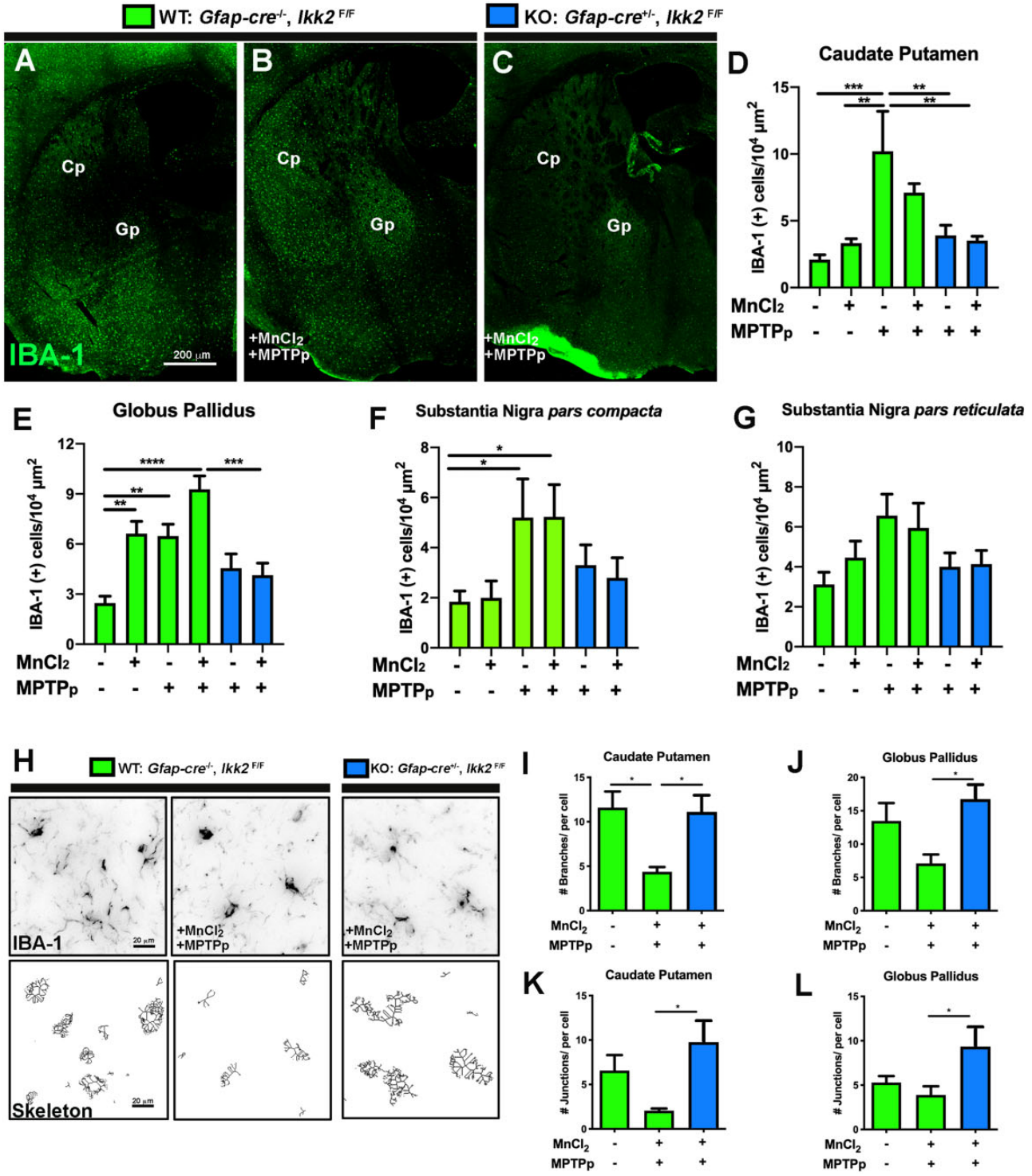

Figure 5. Astrocyte-specific deletion of I kappa B kinase 2 (IKK2) suppresses a reactive phenotype in microglia following sequential exposure to $MnCl_2$ and 1-methyl-4-phenyl-1,2,3,6-tetrahydropyridine (MPTP). The number of microglia in mice sequentially exposed to $MnCl_2$ during juvenile development and to 1-methyl-4-phenyl-1,2,3,6-tetrahydropyridine and probenecid (MPTPp) as adults was analyzed by automated quantitation of tissue sections immunolabeled with anti-IBA1 (green), as depicted in montage images of (A) (wildtype) WT—control, (B) WT—$MnCl_2$/MPTPp, and (C) (knockdown) KO—$MnCl_2$/MPTPp treatment groups. The total number of $IBA1^+$ cells/10^4 μm^2 was quantified in the caudate-putamen (Cp) (D), globus pallidus (Gp) (E), substantia nigra *pars compacta* (F) and substantia nigra *pars reticulata* (G) for all experimental groups ($^*p < .05$; $^{**}p < .01$, $^{***}p < .001$, $^{****}p < .0001$; $N = 5$–6 animals/group). H, Morphological changes in microglia between treatment groups were analyzed by image skeletonization of $IBA1^+$ cells using Image J, as depicted in representative images of WT—Control, WT—$MnCl_2$/MPTPp, and KO—WT + $MnCl_2$/MPTPp. Parameters quantified in each experimental group included the number of branches/cell in Cp/Gp (I, J), and the number of junctions/cell in Cp/Gp (K, L) ($^*p < .05$; $N = 7$ animals/group).

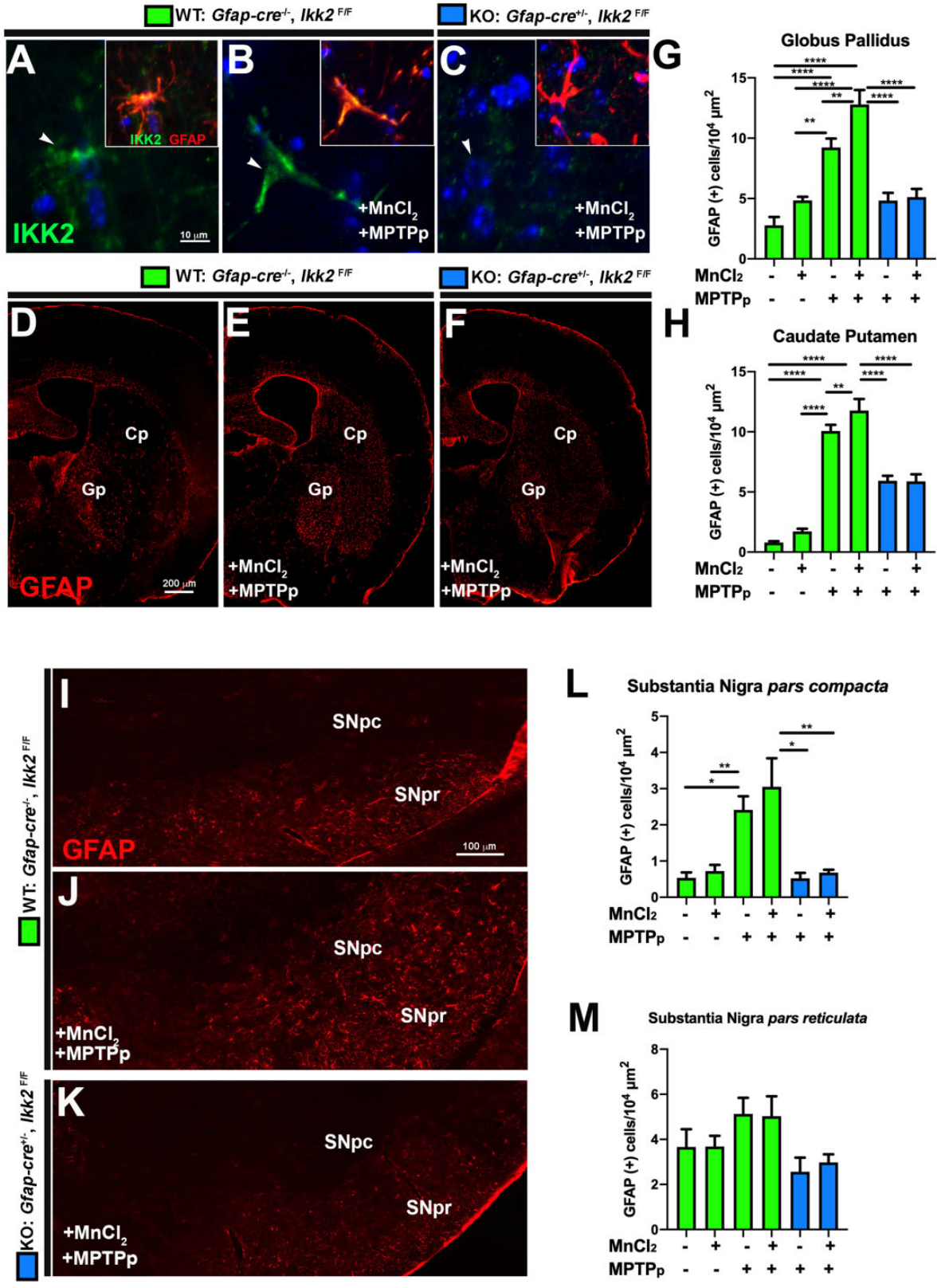

Figure 6. Sequential exposure to $MnCl_2$ and -methyl-4-phenyl-1,2,3,6-tetrahydropyridine and probenecid (MPTPp) during development and adulthood increases astrocyte activation through NF-κB signaling. A–C, High-resolution immunofluorescence images of astrocytes in wildtype (WT) (*Gfap-cre*$^{-/-}$/*Ikk2*$^{F/F}$) and KO (*Gfap-cre*$^{+/-}$/*Ikk2*$^{F/F}$) mice demonstrate expression of I kappa B kinase 2 (IKK2) (green) and glial fibrillary acidic protein (GFAP) (red) that colocalize in WT mice in Control (A) and $MnCl_2$/MPTPp (B) groups, with no detectable expression of IKK in knockout (KO) mice exposed to $MnCl_2$/MPTPp (C). The total number of GFAP$^+$/10^4 μm^2 was quantified in the globus pallidus (Gp) (D) and caudate-putamen (Cp) (H) for each experimental group, as depicted in 10× montage images of the striatum and Gp immunolabeled with anti-GFAP (red) (D–F). Substantia nigra *pars compacta* (SNpc) and substantia nigra *pars reticulata* (SNpr) were also immunostained for GFAP as depicted in representative 10× montage images in (I–K). Analysis of GFAP$^+$/μm^2 in SNpc (L) and SNpr (M) (*$p < .05$, **$p < .01$, ***$p < .001$, ****$p < .0001$; $N = 6$ animals per group).

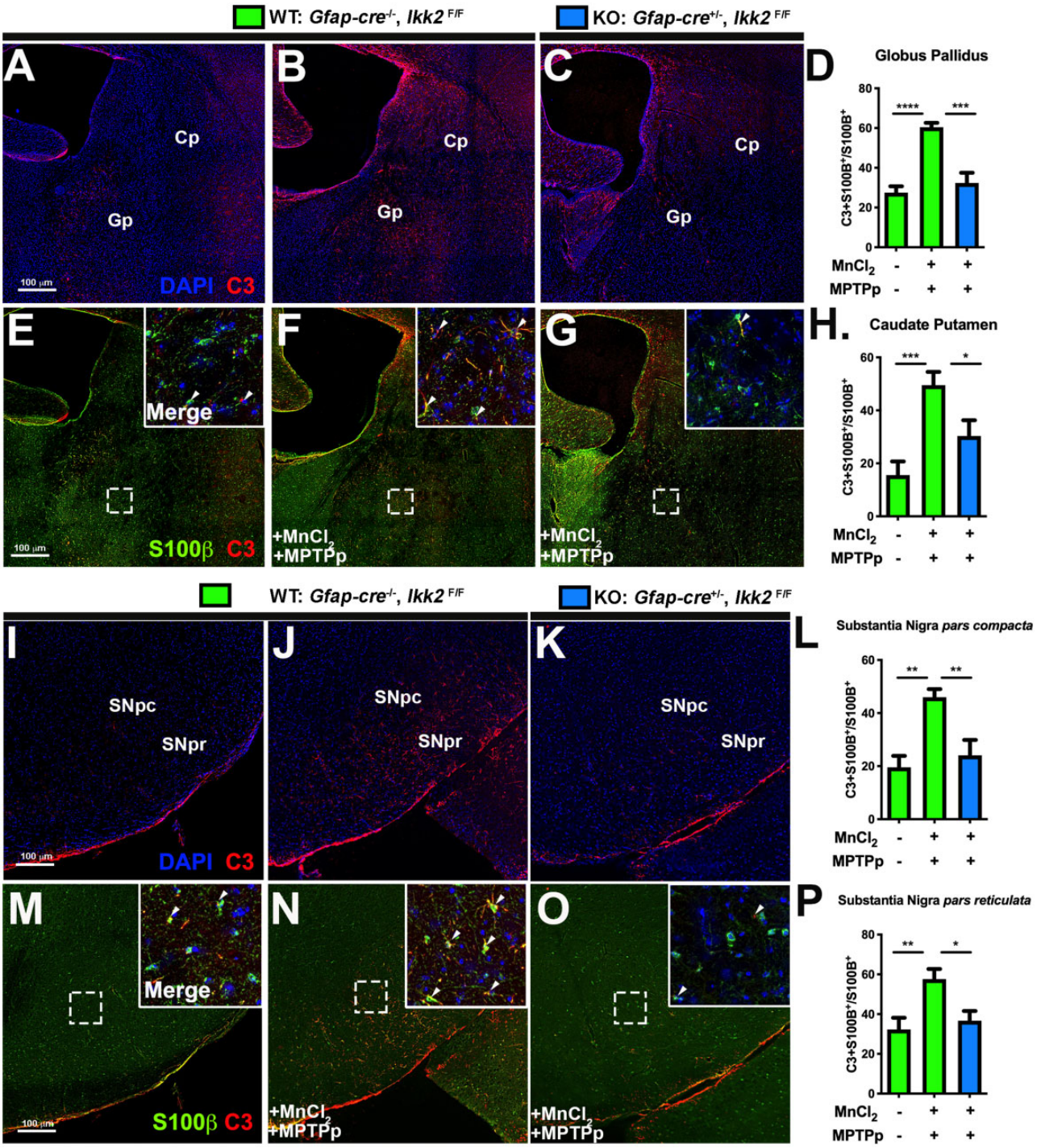

Figure 7. NF-κB signaling regulates the increase in A1 neurotoxic astrocytes in mice sequentially exposed to $MnCl_2$ and methyl-4-phenyl-1,2,3,6-tetrahydropyridine and probenecid (MPTPp). The number of astrocytes coexpressing C3 and S100β was compared with the total number of S100β$^+$ cells in the caudate-putamen (Cp)/globus pallidus (Gp) (A–H) and the substantia nigra (I–P) by immunofluorescence labeling of serial sections through each brain region in wildtype (WT) and knockout (KO) mice. Expression of C3 (red) and S100β (green) was examined in the Cp/Gp in (A) WT—control, (B) WT—$MnCl_2$/MPTPp, and (C) KO—$MnCl_2$/MPTPp treatment groups. Quantification of the number of C3$^+$ + S100β$^+$ cells in each brain region is shown for the Gp (D), Cp (H), substantia nigra *pars compacta* (SNpc) (L), and substantia nigra *pars reticulata* (SNpr) (P) (*$p < .05$, **$p < .01$, ***$p < .001$; $N = 7$ animals/group).

of the complement protein, C3 (Figure 7), which is uniquely expressed in reactive astrocytes of the CNS (Liddelow *et al.*, 2017). S100β was used to determine the total number of astrocytes. Each brain region was imaged using a motorized stage and montage imaging to generate ROIs representing nuclei of interest, including the Cp, Gp, SNpc, and SNpr. The number of astrocytes coexpressing C3$^+$ and S100β$^+$ was compared with the total number of S100β$^+$ cells. WT animals treated with $MnCl_2$/MPTPp exhibited significantly higher numbers of neurotoxic astrocytes in the Gp (Figs. 7B, 7D, and 7F), Cp (Figs. 7B, 7F, and 7H), SNpc (Figs. 7J, 7L, and 7N), and SNpr (Figs. 7J, 7N, and 7P) than control mice. Inhibition of NF-κB signaling in astrocytes in

KO mice suppressed the increase in $C3^+$ astrocytes in each region following treatment with $MnCl_2$/MPTPp, as depicted in the representative images in Figures 7C, 7G, 7K, and 7O ($n = 7$ animals/group; $^*p < .05$, $^{**}p < .01$, $^{***}p < .001$).

DISCUSSION

The pathological mechanisms underlying irreversible neurological damage from Mn exposure are not completely understood. However, neuroinflammatory activation of glial cells is a common mechanism underpinning the neurotoxicity of Mn in both humans and animal models of the disease (Criswell *et al.*, 2018; Kirkley *et al.*, 2017; Moreno *et al.*, 2011). We previously demonstrated that juvenile mice were particularly susceptible to Mn-induced neuroinflammation during the early postweaning period until puberty (PN 21–34) (Moreno *et al.*, 2009a), potentially due to a critical period of striatal development in rodents (Soiza-Reilly and Azcurra, 2009). More recently, we characterized a novel astrocyte-specific transgenic mouse deficient in IKK2, the upstream activating kinase for NF-κB, that prevented inflammatory activation of glial cells loss of dopaminergic neurons in the MPTPp animal model of PD (Kirkley *et al.*, 2019). This study expanded on this work by examining IKK2/NF-κB activation and its role in modulation of neuronal loss and glial reactivity within murine astrocytes following juvenile Mn exposure and secondary exposure to the dopaminergic neurotoxicant MPTP.

Combined developmental/adult exposure to Mn and MPTPp caused considerably different OFT performance compared with the other experimental groups, representing an overall hyperactive phenotype (Figure 4). Behavioral alterations, such as abnormal neuromuscular function and fine motor deficits, have been documented in rat models ranging from low (4.8 mg/kg) subchronic to high (50 mg/kg) chronic $MnCl_2$ administration (Beaudin *et al.*, 2017; Witholt *et al.*, 2000). Dual treatment with $MnCl_2$/MPTPp did not exacerbate DA neuronal loss in the SNpc (Figure 2G) or striatal dopamine production (Figure 4H) over MPTPp alone, suggesting that presynaptic DA neurotransmission is not the major system effected by Mn, in contrast to MPTP. However, Mn increased loss of TH^+ terminals in the Cp in WT mice following dual treatment with MPTPp compared with control and MPTPp-only treatment (Figure 3G). A low, subchronic dose of $MnCl_2$ for 5 weeks also reported little depletion of nigrostriatal DA depletion (Gwiazda *et al.*, 2002). In contrast, Beaudin *et al.* (2017) showed chronic administration of 50 mg/kg/day from PND 20 to 460 significantly depleted DA. Extending $MnCl_2$ treatment in our model longer than 30 days would likely have produced more severe effects on DA levels and DA neuron counts upon exposure to MPTPp.

In the Gp, total $NeuN^+$ neurons in the Gp revealed a trend toward decreased numbers of $NeuN^+$ neurons in mice treated with $MnCl_2$ or MPTPp individually but significant loss of $NeuN^+$ neurons was only detected in $MnCl_2$/MPTPp-treated WT animals compared with controls (Figure 3E). Astrocyte-specific deletion of IKK2 prevented neuronal loss in the Gp, indicating that prior exposure to Mn enhances neuronal injury after a secondary exposure to MPTP through a mechanism involving NF-κB in astrocytes. The extent of Mn-induced glial reactivity may influence the dysregulation of neurotransmitters in the Gp, based in part on the model and dosing regimen. For example, chronic exposure to Mn (10 mg/kg) in nonhuman primates depleted expression of GS in the Gp but had no effect on GABAergic or glutamatergic systems (Burton *et al.*, 2009). Other studies in rats treated with 6 mg/kg/day reported a significant increase in brain Mn levels and a decrease in GABA (Erikson and Aschner, 2003).

The hyperactive locomotor responses observed in Mn-treated mice could also be associated with loss of neurons in the Gp, which would decrease GABAergic output to the Sth and therefore increased Glu excitation to the SNpc and increased firing of DA neurons to the ST through the direct pathway (Erikson and Aschner, 2003). An increase in DA firing could explain modest increases in the number of TH^+ neurons observed in the SNpc in mice treated only with Mn (Figs. 2G and 2H), as well as increases in DA content in the same group (Figure 4H). Serotonergic neurotransmission is also a possible target of Mn toxicity. Alterations in serotonin (5-HT) can cause abnormalities in motor activity and sleep, both of which are symptoms of manganism (Lesch *et al.*, 1996). There was significant increase in the 5-HT metabolite (5-HIAA) of the ST from both dual-treated animal groups, although no differences in levels of 5-HT were detected between groups (Figs. 4L and 4M). This finding is consistent with previous data from our laboratory where we observed that juvenile mice treated with $MnCl_2$ exhibited high levels of 5-HIAA compared with mice treated with Mn only as adults (Moreno *et al.*, 2009b).

Neuronal cell death in response to $MnCl_2$/MPTPp treatment was significantly modulated by IKK2/NF-κB in astrocytes. Inhibition of astrocyte NF-κB signaling in IKK2 KO mice protected DA neurons from both MPTPp and $MnCl_2$/MPTPp-induced toxicity by approximately 90% compared with control within the SNpc (Figure 2G). KO animals also did not sustain any loss of neurons in the Gp and DAergic terminals of the Cp and were similarly preserved (Figs. 3E–G). We previously reported that Mn caused selective apoptosis of interneurons in the striatum and Gp expressing neuronal nitric oxide synthase, enkephalin, and choline acetyl transferase (Liu *et al.*, 2006). Protection against neuronal loss in these brain regions in IKK2 KO mice is consistent with studies reporting that mice with constitutively active astrocyte-NF-κB had increased production of cytokines in the MPTP model of PD, as well as increased amyloid burden and gliosis in a mouse model of AD (Lian *et al.*, 2016; Oeckl *et al.*, 2012). Similarly, KO of IKK2 in all CNS cells demonstrated protection in a mouse model of autoimmune encephalitis (van Loo *et al.*, 2006). The data presented here are the first to report that astrocyte-specific inhibition of IKK2 protects against reactive gliosis and neuronal death induced by combined treatment with $MnCl_2$ and MPTPp.

Astrocyte-specific deletion of IKK2 also reduced microglial activation in the Gp (Figs. 5E, 5J, and 5L) and Cp (Figs. 5D, 5I, and 5K), suggesting that cell-cell signaling in glia is critical to achieving a neurotoxic inflammatory response. Inhibition of microglial activation in the Gp of KO animals directly correlated with the preservation of $NeuN^+$ cells with dual treatment (Figs. 3E and 5E). However, no significant suppression of microgliosis was observed in the SNpc or SNpr, consistent with the initial characterization of hGFAP-$cre^{+/-}$/$IKK2^{fl/fl}$ treated with MPTPp (Figs. 5F and 5G) (Kirkley *et al.*, 2019). Microglia stimulate phenotypic activation of neurotoxic A1 astrocytes through release of factors such as TNFα, C1q, and IL1α (Liddelow *et al.*, 2017) that in turn further magnify microglial reactivity through NF-κB-dependent production of neuroinflammatory signaling molecules such as CCL2 (Popichak *et al.*, 2018). Thus, dampening innate immune inflammatory signaling in astrocytes through gene deletion of IKK2 likely prevented more severe neuroinflammatory activation of microglia in this model. We previously reported that immunopurified primary astrocytes isolated from IKK2 KO mice exhibited 70% knockdown of IKK2 (Kirkley *et al.*, 2019),

which we also observed here, as depicted in representative images of IKK2/GFAP colocalization in Figures 6A–C. Quantitation of the number of $GFAP^+$ cells/μm^2 confirmed that the Gp was most effected nucleus in WT mice exposed to Mn/MPTPp (Figs. 6D and 6F). KO animals exhibited significantly fewer $GFAP^+$ cells/μm^2 in the Gp, Cp, and SNpc, although no groups were different in the SNpr, potentially due to constitutively high basal levels of astrocytes present in this brain region (Figs. 6D–M).

Notably, no increases in Mn were observed in astrocyte-specific IKK2 KO mice following Mn treatment at PN 51 in the SN, striatum or in the cortex, although basal levels were somewhat higher in these brain regions (Figs. 1D–F). This suggested that decreased neurotoxicity in KO mice following MPTP treatment in Mn-exposed mice could be due in part to less accumulation of Mn in the brain. We therefore measured mRNA levels of several metal transporters known to regulate Mn and uptake and neurotoxicity, including *Slc11a2* (*Dmt1*), *Slc39a8* (*Zip8*), *Slc39a10*, and *Slc39a14* (Figs. 1H–M). There were no differences amongst these metal transporters in the SN between WT and KO mice, although levels of *Dmt1* were increased in the cortex following dual treatment with Mn + MPTP. Expression of *Slc39a8* was very low in all brain regions and did not change between genotype and treatment condition, consistent with patterns of expression previously reported (Yue *et al.*, 2014). Both DMT1 and SLC39A10 are important transporters for Mn in the periphery and in brain (Illing *et al.*, 2012; Taylor *et al.*, 2019) and SLC39A10 is protective against Mn neurotoxicity (Illing *et al.*, 2012). DMT1 is at least partly regulated by NF-κB (Paradkar and Roth, 2006) and induced in neurons during exposure to MPTP (Xu *et al.*, 2010). An increase in DMT1 could therefore modulate neurotoxicity but despite higher baseline levels of Mn in KO mice compared with WT in each brain region, deletion of IKK2 in astrocytes still protected against neuronal injury from dual treatment with Mn + MPTP. These data suggest that altered accumulation of Mn in KO mice is not primarily responsible for the observed degree of neuroprotection. Treatment with Mn up to 100 mg/kg results in an apparent saturation point in the brain following oral exposure in mice (Liu *et al.*, 2006; Moreno *et al.*, 2009b), so it is likely that IKK2 inhibition would suppress innate immune inflammatory responses across a range of Mn concentrations.

However, astrocyte-specific deletion of IKK2 prevented MPTP-induced neuronal loss and glial activation even in the absence of Mn exposure, suggesting that attenuating innate immune inflammatory responses in this cell type was directly neuroprotective. Moreover, levels of Mn were similar between genotypes in all groups at the time of treatment with MPTP, indicating that differences in metal transporters were likely not the primary drivers of later neuronal loss in dual-treated animals. However, even slight increases in Mn can have lasting effects on levels of biogenic amines in the striatum (Lasley *et al.*, 2020), suggesting that altered states of glial activation could persist even after Mn was excreted, perhaps due to epigenetic imprinting during the juvenile exposure period. Such mechanisms remained to be elucidated in subsequent studies.

Studies of MPTP neurotoxicity demonstrate that microglia quickly activate following MPTP exposure and trigger a sustained inflammatory phenotype in astrocytes (Hirsch and Hunot, 2009; Huang *et al.*, 2018). To detect neurotoxic A1 astrocytes, we immunolabeled for complement protein-C3 (Figure 7), a component of the classical complement pathway mediating innate immune responses to pathogens (Ricklin *et al.*, 2016) that is uniquely expressed in reactive A1 astrocytes, not in resting A2 astrocytes (Liddelow *et al.*, 2017; Nitkiewicz *et al.*, 2017). C3 is an NF-κB-regulated gene in astrocytes (Lian *et al.*, 2016; Nitkiewicz *et al.*, 2017) that is increased in mouse models of AD (Lian *et al.*, 2016). We observed that IKK2 KO mice had fewer $C3^+$ A1 astrocytes after dual exposure to $MnCl_2$/MPTPp treatment compared with the WT animals (Figs. 7D, 7H, 7L, and 7P) suggesting that astrocyte-NF-κB regulated C3 expression may be an important mechanism to stimulate neuroinflammation and neurodegeneration following 2-hit exposure to Mn and MPTP.

In conclusion, we report a neuroinflammatory mechanism in astrocytes associated with juvenile $MnCl_2$ exposure that exacerbated neurodegeneration from later adult exposure to MPTPp. These data demonstrate that astrocyte-specific gene deletion of NF-κB/IKK2 mitigates the numbers of reactive astrocytes and microglia and protects against neuronal loss in the basal ganglia induced by sequential exposure to Mn and MPTPp.

FUNDING

National Institutes of Health (R01ES021656, R01ES030937 to R.B.T., F31ES026860 to K.A.P., F31NS096841 to S.L.H.).

DECLARATION OF CONFLICTING INTERESTS

The authors declared no potential conflicts of interest with respect to the research, authorship, and/or publication of this article.

REFERENCES

Aschner, M., Erikson, K. M., Herrero Hernandez, E., and Tjalkens, R. (2009). Manganese and its role in Parkinson's disease: From transport to neuropathology. *Neuromol. Med.* **11**, 252–266.

Beaudin, S. A., Strupp, B. J., Strawderman, M., and Smith, D. R. (2017). Early postnatal manganese exposure causes lasting impairment of selective and focused attention and arousal regulation in adult rats. *Environ. Health Perspect.* **125**, 230–236.

Brown, T. P., Rumsby, P. C., Capleton, A. C., Rushton, L., and Levy, L. S. (2006). Pesticides and Parkinson's disease—Is there a link? *Environ. Health Perspect.* **114**, 156–164.

Burton, N. C., Schneider, J. S., Syversen, T., and Guilarte, T. R. (2009). Effects of chronic manganese exposure on glutamatergic and GABAergic neurotransmitter markers in the non-human primate brain. *Toxicol. Sci.* **111**, 131–139.

Criswell, S. R., Warden, M. N., Searles Nielsen, S., Perlmutter, J. S., Moerlein, S. M., Sheppard, L., Lenox-Krug, J., Checkoway, H., and Racette, B. A. (2018). Selective D2 receptor PET in manganese-exposed workers. *Neurology* **91**, e1022–1030.

Erikson, K. M., and Aschner, M. (2003). Manganese neurotoxicity and glutamate-GABA interaction. *Neurochem. Int.* **43**, 475–480.

Glass, C. K., Saijo, K., Winner, B., Marchetto, M. C., and Gage, F. H. (2010). Mechanisms underlying inflammation in neurodegeneration. *Cell* **140**, 918–934.

Gouveia, K., and Hurst, J. L. (2013). Reducing mouse anxiety during handling: Effect of experience with handling tunnels. *PLoS One* **8**, e66401.

Guilarte, T. R., Chen, M. K., McGlothan, J. L., Verina, T., Wong, D. F., Zhou, Y., Alexander, M., Rohde, C. A., Syversen, T., Decamp, E., *et al.* (2006). Nigrostriatal dopamine system dysfunction and subtle motor deficits in manganese-exposed non-human primates. *Exp. Neurol.* **202**, 381–390.

Gwiazda, R. H., Lee, D., Sheridan, J., and Smith, D. R. (2002). Low cumulative manganese exposure affects striatal GABA but not dopamine. *Neurotoxicology* **23**, 69–76.

Hammond, S. L., Popichak, K. A., Li, X., Hunt, L. G., Richman, E. H., Damale, P. U., Chong, E. K. P., Backos, D. S., Safe, S., and Tjalkens, R. B. (2018). The Nurr1 ligand, 1,1-bis(3′-indolyl)-1-(p-chlorophenyl)methane, modulates glial reactivity and is neuroprotective in MPTP-induced parkinsonism. *J. Pharmacol. Exp. Ther.* **365**, 636–651.

He, P., Liu, D. H., and Zhang, G. Q. (1994). [Effects of high-level-manganese sewage irrigation on children's neurobehavior]. *Zhonghua Yu Fang Yi Xue Za Zhi* **28**, 216–218.

Hirsch, E. C., and Hunot, S. P. (2009). Neuroinflammation in Parkinson's disease: A target for neuroprotection? *Lancet Neurol.* **8**, 382–397.

Huang, D., Wang, Z., Tong, J., Wang, M., Wang, J., Xu, J., Bai, X., Li, H., Huang, Y., Wu, Y., *et al.* (2018). Long-term changes in the nigrostriatal pathway in the MPTP mouse model of Parkinson's disease. *Neuroscience* **369**, 303–313.

Illing, A. C., Shawki, A., Cunningham, C. L., and Mackenzie, B. (2012). Substrate profile and metal-ion selectivity of human divalent metal-ion transporter-1. *J. Biol. Chem.* **287**, 30485–30496.

Kirkley, K. S., Popichak, K. A., Afzali, M. F., Legare, M. E., and Tjalkens, R. B. (2017). Microglia amplify inflammatory activation of astrocytes in manganese neurotoxicity. *Neuroinflammation* **14**, 99.

Kirkley, K. S., Popichak, K. A., Hammond, S. L., Davies, C., Hunt, L., and Tjalkens, R. B. (2019). Genetic suppression of IKK2/NF-κB in astrocytes inhibits neuroinflammation and reduces neuronal loss in the MPTP-probenecid model of Parkinson's disease. *Neurobiol. Dis.* **127**, 193–209.

Lasley, S. M., Fornal, C. A., Mandal, S., Strupp, B. J., Beaudin, S. A., and Smith, D. R. (2020). Early postnatal manganese exposure reduces rat cortical and striatal biogenic amine activity in adulthood. *Toxicol. Sci.* **173**, 144–155.

Lesch, K. P., Bengel, D., Heils, A., Sabol, S. Z., Greenberg, B. D., Petri, S., Benjamin, J., Müller, C. R., Hamer, D. H., and Murphy, D. L. (1996). Association of anxiety-related traits with a polymorphism in the serotonin transporter gene regulatory region. *Science* **274**, 1527–1531.

Lian, H., Litvinchuk, A., Chiang, A. C. A., Aithmitti, N., Jankowsky, J. L., and Zheng, H. (2016). Astrocyte-microglia cross talk through complement activation modulates amyloid pathology in mouse models of Alzheimer's disease. *J. Neurosci.* **36**, 577–589.

Liddelow, S. A., Guttenplan, K. A., Clarke, L. E., Bennett, F. C., Bohlen, C. J., Schirmer, L., Bennett, M. L., Münch, A. E., Chung, W.-S., Peterson, T. C., *et al.* (2017). Neurotoxic reactive astrocytes are induced by activated microglia. *Nat. Publishing Group* **541**, 481–487.

Liu, X., Sullivan, K. A., Madl, J. E., Legare, M., and Tjalkens, R. B. (2006). Manganese-induced neurotoxicity: The role of astroglial-derived nitric oxide in striatal interneuron degeneration. *Toxicol. Sci.* **91**, 521–531.

Mergler, D., and Baldwin, M. (1997). Early manifestations of manganese neurotoxicity in humans: An update. *Environ. Res.* **73**, 92–100.

Miller, J. A., Runkle, S. A., Tjalkens, R. B., and Philbert, M. A. (2011). 1,3-Dinitrobenzene-induced metabolic impairment through selective inactivation of the pyruvate dehydrogenase complex. *Toxicol. Sci.* **122**, 502–511.

Moreno, J. A., Streifel, K. M., Sullivan, K. A., Hanneman, W. H., and Tjalkens, R. B. (2011). Manganese-induced NF-kappaB activation and nitrosative stress is decreased by estrogen in juvenile mice. *Toxicol. Sci.* **122**, 121–133.

Moreno, J. A., Streifel, K. M., Sullivan, K. A., Legare, M. E., and Tjalkens, R. B. (2009a). Developmental exposure to manganese increases adult susceptibility to inflammatory activation of glia and neuronal protein nitration. *Toxicol. Sci.* **112**, 405–415.

Moreno, J. A., Yeomans, E. C., Streifel, K. M., Brattin, B. L., Taylor, R. J., and Tjalkens, R. B. (2009b). Age-dependent susceptibility to manganese-induced neurological dysfunction. *Toxicol. Sci.* **112**, 394–404.

Morrison, H. W., and Filosa, J. A. (2013). A quantitative spatiotemporal analysis of microglia morphology during ischemic stroke and reperfusion. *J. Neuroinflamm.* **10**, 1–1.

Nitkiewicz, J., Borjabad, A., Morgello, S., Murray, J., Chao, W., Emdad, L., Fisher, P. B., Potash, M. J., and Volsky, D. J. (2017). HIV induces expression of complement component C3 in astrocytes by NF-κB-dependent activation of interleukin-6 synthesis. *J. Neuroinflamm.* **14**, 23.

Oeckl, P., Lattke, M., Wirth, T., Baumann, B., and Ferger, B. (2012). Astrocyte-specific IKK2 activation in mice is sufficient to induce neuroinflammation but does not increase susceptibility to MPTP. *Neurobiol. Dis.* **48**, 481–487.

Paradkar, P. N., and Roth, J. A. (2006). Nitric oxide transcriptionally down-regulates specific isoforms of divalent metal transporter (DMT1) via NF-kappaB. *J. Neurochem.* **96**, 1768–1777.

Peres, T. V., Schettinger, M. R., Chen, P., Carvalho, F., Avila, D. S., Bowman, A. B., and Aschner, M. (2016). "Manganese-induced neurotoxicity: A review of its behavioral consequences and neuroprotective strategies". *BMC Pharmacol. Toxicol.* **17**, 57.

Popichak, K. A., Afzali, M. F., Kirkley, K. S., and Tjalkens, R. B. (2018). Glial-neuronal signaling mechanisms underlying the neuroinflammatory effects of manganese. *J. Neuroinflamm.* **15**, 324.

Racette, B. A., Searles Nielsen, S., Criswell, S. R., Sheppard, L., Seixas, N., Warden, M. N., and Checkoway, H. (2017). Dose-dependent progression of parkinsonism in manganese-exposed welders. *Neurology* **88**, 344–351.

Ricklin, D., Reis, E. S., Mastellos, D. C., Gros, P., and Lambris, J. D. (2016). Complement component C3—The 'Swiss Army Knife' of innate immunity and host defense. *Immunol. Rev.* **274**, 33–58.

Rodier, J. (1955). Manganese poisoning in Moroccan miners. *Br. J. Ind. Med.* **12**, 21–35.

Rugless, F., Bhattacharya, A., Succop, P., Dietrich, K. N., Cox, C., Alden, J., Kuhnell, P., Barnas, M., Wright, R., Parsons, P. J., *et al.* (2014). Childhood exposure to manganese and postural instability in children living near a ferromanganese refinery in Southeastern Ohio. *Neurotoxicol. Teratol.* **41**, 71–79.

Schneider, C. A., Rasband, W. S., and Eliceiri, K. W. (2012). NIH image to ImageJ: 25 years of image analysis. *Nat. Methods* **9**, 671–675.

Soiza-Reilly, M., and Azcurra, J. M. (2009). Developmental striatal critical period of activity-dependent plasticity is also a window of susceptibility for haloperidol induced adult motor alterations. *Neurotoxicol. Teratol.* **31**, 191–197.

Stuart, S. A., and Robinson, E. S. (2015). Reducing the stress of drug administration: Implications for the 3Rs. *Sci. Rep.* **5**, 14288.

Takser, L., Mergler, D., Hellier, G., Sahuquillo, J., and Huel, G. (2003). Manganese, monoamine metabolite levels at birth, and child psychomotor development. *Neurotoxicology* **24**, 667–674.

Tapias, V., Greenamyre, J. T., and Watkins, S. C. (2013). Automated imaging system for fast quantitation of neurons, cell morphology and neurite morphometry *in vivo* and *in vitro*. *Neurobiol. Dis.* **54**, 158–168.

Taylor, C. A., Hutchens, S., Liu, C., Jursa, T., Shawlot, W., Aschner, M., Smith, D. R., and Mukhopadhyay, S. (2019). SLC30A10 transporter in the digestive system regulates brain manganese under basal conditions while brain SLC30A10 protects against neurotoxicity. *J. Biol. Chem.* **294**, 1860–1876.

van Loo, G., De Lorenzi, R., Schmidt, H., Huth, M., Mildner, A., Schmidt-Supprian, M., Lassmann, H., Prinz, M. R., and Pasparakis, M. (2006). Inhibition of transcription factor NF-κB in the central nervous system ameliorates autoimmune encephalomyelitis in mice. *Nat. Immunol.* **7**, 954–961.

Wang, J. D., Huang, C. C., Hwang, Y. H., Chiang, J. R., Lin, J. M., and Chen, J. S. (1989). Manganese induced parkinsonism: An outbreak due to an unrepaired ventilation control system in a ferromanganese smelter. *Br. J. Ind. Med.* **46**, 856–859.

Witholt, R., Gwiazda, R. H., and Smith, D. R. (2000). The neurobehavioral effects of subchronic manganese exposure in the presence and absence of pre-parkinsonism. *Neurotoxicol. Teratol.* **22**, 851–861.

Xu, H., Jiang, H., Wang, J., and Xie, J. (2010). Rg1 protects the MPP+-treated MES23.5 cells via attenuating DMT1 up-regulation and cellular iron uptake. *Neuropharmacology* **58**, 488–494.

Yue, F., Cheng, Y., Breschi, A., Vierstra, J., Wu, W., Ryba, T., Sandstrom, R., Ma, Z., Davis, C., Pope, B. D., *et al.* (2014). A comparative encyclopedia of DNA elements in the mouse genome. *Nature* **515**, 355–364.

Zidenberg-Cherr, S., Keen, C. L., Lonnerdal, B., and Hurley, L. S. (1983). Superoxide dismutase activity and lipid peroxidation in the rat: Developmental correlations affected by manganese deficiency. *J. Nutr.* **113**, 2498–2504.